

A FINITE VOLUME METHOD PRESERVING MAXIMUM PRINCIPLE FOR THE CONJUGATE HEAT TRANSFER PROBLEMS WITH GENERAL INTERFACE CONDITIONS*

Huifang Zhou

School of Mathematics, Jilin University, Changchun 130012, China

The Graduate School of China Academy of Engineering Physics, Beijing 100088, China

Email: 13614405274@163.com

Zhiqiang Sheng

Laboratory of Computational Physics, Institute of Applied Physics and Computational Mathematics, Beijing 100088, China

HEDPS, Center for Applied Physics and Technology, and College of Engineering, Peking University, Beijing 100871, China

Email: sheng_zhiqiang@iapcm.ac.cn

Guangwei Yuan¹⁾

Laboratory of Computational Physics, Institute of Applied Physics and Computational Mathematics, Beijing 100088, China

Email: yuan_guangwei@iapcm.ac.cn

Abstract

In this paper, we present a unified finite volume method preserving discrete maximum principle (DMP) for the conjugate heat transfer problems with general interface conditions. We prove the existence of the numerical solution and the DMP-preserving property. Numerical experiments show that the nonlinear iteration numbers of the scheme in [24] increase rapidly when the interfacial coefficients decrease to zero. In contrast, the nonlinear iteration numbers of the unified scheme do not increase when the interfacial coefficients decrease to zero, which reveals that the unified scheme is more robust than the scheme in [24]. The accuracy and DMP-preserving property of the scheme are also verified in the numerical experiments.

Mathematics subject classification: 65M08, 35K59.

Key words: Conjugate heat transfer problems, General interface conditions, Finite volume scheme, Discrete maximum principle.

1. Introduction

The conjugate heat transfer refers to the phenomenon of thermal interaction between different materials with different temperature. The problems are often illustrated by elliptic or parabolic interface problems in partitioned domain, in which the interface represents where the contact occurs. The conjugate heat transfer arises widely in physics and engineering, such as the modeling of heat transfer through multilayered walls in buildings, electronics packaging, heat exchangers, space craft structures and nuclear reactor [15], etc.

Thermal properties of different materials, such as thermal conductivity, heat capacity, and density, are usually different, which causes discontinuity of diffusion coefficients across the

* Received October 4, 2020 / Revised version received March 5, 2021 / Accepted July 2, 2021 /
Published online August 9, 2022 /

¹⁾ Corresponding author

interface. Across the interface, these problems also impose the temperature and the conductive heat flux satisfying certain interface conditions. According to the interface conditions, the elliptic interface problems can be divided into the following two types.

The most common problems are the perfect interface problems, in which both the temperature and the conductive heat flux are required to be continuous. The corresponding conditions are called perfect interface conditions. This kind of problems is usually solved as an overall problems on the whole domain. There have been many researches concerning about this problem, such as finite difference methods [9], finite element methods [12, 25], finite volume methods [14, 17, 18, 21], and discontinuous Galerkin (DG) methods [5, 13, 22], and so on.

The other type is the imperfect interface problems. When the two materials are relatively sliding, there exists interfacial heat resistance, which is called Kapitza resistance, impeding the heat transfer across the interface. In this case, the conductive heat flux is still conservative, while the temperature is discontinuous because of the roughness of the interface. The model of perfect interface problems is not suitable for such kind of problems any more. For this type of problems, the jump of temperature is usually in proportion to the normal heat flux, which is known as imperfect interface conditions. Moreover, the proportion is denoted by $\mu(\mathbf{x})$ in the rest of paper, which is always non-negative. The coefficient is also called interfacial thermal resistance coefficient or Kapitza coefficient.

Many numerical methods only concern about problems with positive interfacial coefficient $\mu > 0$, such as finite element methods [8, 10], finite difference methods [3], finite volume methods [2, 4, 24], DG Methods [1, 7]. For the finite element methods, a DMP-preserving method [8] and a nonstandard variation form [10] are proposed. For the finite volume methods, high-order scheme [4], positivity-preserving scheme [24] and DMP-preserving scheme [2] are studied, respectively. An interior-penalty DG method [1] and local DG Method [7] are presented.

However, the actual materials on interface may be variant, therefore the corresponding interfacial coefficients may be zero somewhere and non-zero elsewhere. On one hand, the coefficient matrices of schemes designed for imperfect interface problems [1–4, 7, 8, 10, 24] are close to singular when the interfacial coefficients tend to zero, which leads to efficiency decrease of the scheme. On the other hand, the above schemes are ill-posed for the perfect interface problems when interfacial coefficients degenerate to zero somewhere. Based on the above considerations, it is crucial to propose a unified scheme to deal with the interface problems with general contact conditions, which means that the scheme is effective both for the perfect interface problems and the imperfect interface problems. Unfortunately, limited work has been done in unified discretization for such problems. To the best of our knowledge, the unified scheme for general interfacial coefficient is only proposed in [16, 19, 20]. A non-traditional finite element method is proposed on non-body-fitting grids in [19]. A special iterative method which is robust with respect to the interfacial coefficient is designed in [20]. In [16], both continuous variational formulation and the finite element method are considered, and the numerical results are compared with the real optical micrograph. There also exist some researches concerning other types of interface problem, where the jumps of solution and flux on the interface are given functions. In [11], a finite difference method is proposed on Cartesian grids. In [6], a symmetric discontinuous Galerkin method is studied on fitted meshes, and the high-order convergence is proved.

The maximum principle is an essential property for the conjugate heat transfer problems and it reveals physical restriction of unknowns, such as temperature. If a numerical scheme does not preserve the DMP, it may produce non-physical oscillation and even cause calculation

interruption. Besides, it may violate the second law of thermodynamics. For the interface problems, as far as we know, the DMP is only discussed in [24] and [8]. However, the schemes in [8, 24] can only be applied to positive interfacial coefficient and triangular meshes, and can not deal with the perfect interface problems. Most importantly, the efficiency of the schemes in [8, 24] decreases when the interfacial coefficients are very small. Therefore, it is necessary to propose a robust DMP-preserving scheme for the conjugate heat transfer problems with general interfacial coefficients.

In this work, we propose a unified DMP-preserving finite volume scheme on general polygonal meshes for solving conjugate heat transfer problems with general interface conditions. The unified scheme has the following advantages:

- The scheme is valid for general interface problems, i.e., the interfacial coefficient can be nonnegative.
- The discrete maximum principle is preserved.
- The conservation of heat flux is preserved.
- The polygonal meshes can be used.

The existence of numerical solution is proved, as well as the property that there exists a subsequence of numerical solutions for imperfect interface problems converging to the numerical solution for perfect interface problems as the interfacial coefficients tending to zero uniformly is proved. Moreover, in the numerical experiments, the proposed scheme and the scheme in [24] are compared under different interfacial coefficients. For positive interfacial coefficients $\mu > 0$, we observe that the nonlinear iteration numbers of scheme in [24] increase rapidly as the coefficients tending to zero, although second order convergence is obtained. Meanwhile, the iteration numbers of the proposed scheme do not remarkably increase and second order convergence is also obtained. For interfacial coefficient $\mu(\mathbf{x}) = 0$ for some point $\mathbf{x} \in \Gamma$, the scheme in [24] loses accuracy, meanwhile the proposed scheme can obtain second order accuracy. Simultaneously, the iteration numbers are relatively few. The second order accuracy of the scheme is verified on different shaped interfaces, such as straight line, circle, and sinusoid. The numerical experiments verify that our scheme is DMP-preserving and effective for general interface problems, which is more robust than the scheme in [24]. In conclusion, the improvements of this paper compared to [24] are as follows:

- The physical background of this paper is more general. It allows the interfacial coefficient to be zero or very close to zero.
- For the problem with small interfacial coefficient, the scheme in this paper improves the efficiency greatly. When the minimum of μ is magnitude of 1E-4, numerical results show that the nonlinear iteration number of [24] is almost 140 times on average of that in this paper.

The main distinction between the unified scheme and the scheme in [24] is the discretization for interface conditions. The discretization is specially designed to deal with the problem with general interface conditions in this paper. Besides, the nonlinear iteration methods are different. Robin-Robin iteration is employed in [24]. The Picard iteration is employed directly in this paper.

An outline of this paper is as follows. The interface problems with general interfacial coefficient are introduced in Section 2. The DMP-preserving finite volume scheme is constructed in Section 3. In Section 4, we prove the DMP-preserving property and existence of numerical solution, and prove that there exists a subsequence of the numerical solution for imperfect interface problems converging to the numerical solution for perfect interface problems. Some numerical experiments are presented in Section 5, showing that our proposed scheme is more robust than the scheme in [24] and verifying the DMP-preserving property. Finally, a brief summery is given in Section 6.

2. The Model Problem

Consider the conjugate heat transfer problems with general interface condition on domain Ω presented in Fig. 2.1. Ω_1 and Ω_2 represent two disjoint subdomains where two different materials located, and Γ represents the contact interface between different materials. We denote \mathbf{n}_1 the outward unit normal vector of Ω_1 on interface $\partial\Omega_1 \cap \Gamma$ and denote \mathbf{n}_2 the outward unit normal vector of Ω_2 on interface $\partial\Omega_2 \cap \Gamma$. The general interface condition imposes the normal heat flux to be continuous and the jump of solution to be in proportion to the continuous normal heat flux on the interface. The model problem has the following form:

$$-\nabla \cdot (\kappa_1(\mathbf{x})\nabla u_1(\mathbf{x})) = f(\mathbf{x}), \quad \text{in } \Omega_1, \quad (2.1)$$

$$-\nabla \cdot (\kappa_2(\mathbf{x})\nabla u_2(\mathbf{x})) = f(\mathbf{x}), \quad \text{in } \Omega_2, \quad (2.2)$$

$$u_1(\mathbf{x}) = g(\mathbf{x}), \quad \text{on } \partial\Omega_1 \setminus \Gamma, \quad (2.3)$$

$$u_2(\mathbf{x}) = g(\mathbf{x}), \quad \text{on } \partial\Omega_2 \setminus \Gamma, \quad (2.4)$$

$$u_2(\mathbf{x}) - u_1(\mathbf{x}) = \mu(\mathbf{x})\kappa_1(\mathbf{x})\nabla u_1(\mathbf{x}) \cdot \mathbf{n}_1, \quad \text{on } \Gamma, \quad (2.5)$$

$$\kappa_1(\mathbf{x})\nabla u_1(\mathbf{x}) \cdot \mathbf{n}_1 = -\kappa_2(\mathbf{x})\nabla u_2(\mathbf{x}) \cdot \mathbf{n}_2, \quad \text{on } \Gamma, \quad (2.6)$$

where κ_1 and κ_2 are the positive definite diffusion tensors on Ω_1 and Ω_2 , respectively, $f(\mathbf{x}) \in L^2(\Omega)$ and $g(\mathbf{x}) \in H^{1/2}(\partial\Omega)$. The interfacial coefficient satisfies $\mu(\mathbf{x}) \geq 0$, which is more general than the case $\mu(\mathbf{x}) > 0$ in [1–4, 7, 8, 10, 24].

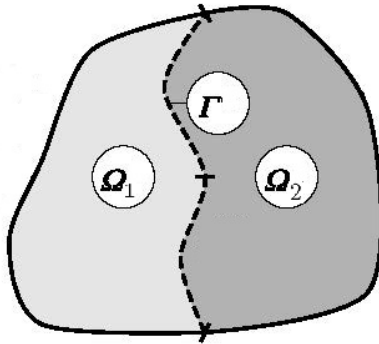


Fig. 2.1. The domain and the interface.

For the interface problem with general conditions (2.1)-(2.6), the maximum principle is demonstrated in the following theorem, whose proof can be found in [8].

Theorem 2.1. *Suppose $u \in C^2(\Omega_i) \cap C^1(\bar{\Omega}_i)$ ($i = 1, 2$) is the solution of (2.1)-(2.6), then we have:*

(i) *Suppose $f(\mathbf{x}) \geq 0$, if $u(\mathbf{x})$ is not a constant on $\bar{\Omega}$, then the minimum of $u(\mathbf{x})$ on $\bar{\Omega}$ can only be attained on $\partial\Omega$.*

(ii) *Suppose $f(\mathbf{x}) \leq 0$, if $u(\mathbf{x})$ is not a constant on $\bar{\Omega}$, then the maximum of $u(\mathbf{x})$ on $\bar{\Omega}$ can only be attained on $\partial\Omega$.*

(iii) *Suppose $f(\mathbf{x}) = 0$, if $u(\mathbf{x})$ is not a constant on $\bar{\Omega}$, then the maximum and minimum of $u(\mathbf{x})$ on $\bar{\Omega}$ can only be attained on $\partial\Omega$.*

3. The Finite Volume Scheme Preserving DMP

In this section, we will construct the finite volume scheme preserving DMP for the interface problem with general interface conditions (2.1)-(2.6).

In Section 3.1, we introduce some notations. In Section 3.2 and Section 3.3, the constructions for numerical unilateral heat flux and conservative flux are illustrated. The constructions in Section 3.2 and Section 3.3 are the same as Section 3.1 and Section 3.2 in [24], so we just present the final expressions. In Section 3.4, the discretization of the interface condition is given. The discretization of interface condition in this paper is different from that in [24], and is the key to deal with general interfacial coefficient $\mu \geq 0$. In Section 3.5, the resulting finite volume scheme is proposed, which is also different from the scheme in [24] because of the different discretization of interface condition.

3.1. Preliminaries

First, we need to introduce some notations, which are displayed in Fig. 3.1 and listed in Table 3.1, respectively. In the notations, the subscript i represents different subdomains, and i can be either 1 or 2.

Table 3.1: The notations.

Notation	Meaning
\mathcal{J}_i	the set of cells on Ω_i
\mathcal{J}	the union of $\mathcal{J}_1 \cup \mathcal{J}_2$
\mathcal{J}_i^{out}	the set of degenerated “ghost” cells on boundary $\partial\Omega_i \setminus \Gamma$
\mathcal{J}^{out}	the union of $\mathcal{J}_1^{out} \cup \mathcal{J}_2^{out}$
\mathcal{J}_i^Γ	the set of degenerated “ghost” cells on interface Γ in Ω_i
\mathcal{J}^Γ	the union of $\mathcal{J}_1^\Gamma \cup \mathcal{J}_2^\Gamma$
\mathcal{E}_i	the set of all the cell edges of Ω_i
\mathcal{E}	the union of $\mathcal{E}_1 \cup \mathcal{E}_2$
K	a cell in \mathcal{J} , also represents the cell center
L	the adjacent cell of K , also represents the cell center
σ	the common edge of cells K and L
\mathcal{E}_K	the set of edges of cell K

For the “ghost” cells on boundary and interface, we add further explanations here. On the boundary and interface, K is an edge on $\partial\Omega_i \setminus \Gamma$ instead of a polygon. The reason why we introduce “ghost cells” is that the exact solution is discontinuous across Γ , and the “ghost cells” shall play an important role in the construction of the scheme.

Denote by $\mathbf{n}_{K\sigma}$ the unit outward normal vector of cell K on edge σ and $\mathbf{n}_{L\sigma}$ the unit outward normal vector of cell L on edge σ . A ray originating at the point K along the direction $\kappa_1^T \mathbf{n}_{K\sigma}$ (or $\kappa_2^T \mathbf{n}_{K\sigma}$) must intersect with one segment connecting two neighboring midpoints of the edge of cell K , two midpoints are denoted by M_1 and M_2 , the cross point is denoted by O_1 . θ_{K_1} is the angle between KO_1 and KM_1 , and θ_{K_2} is the angle between KO_1 and KM_2 . Denote $\theta_K = \theta_{K_1} + \theta_{K_2}$. Similarly, a ray originating at the point L along the direction $\kappa_1^T \mathbf{n}_{L\sigma}$ (or $\kappa_2^T \mathbf{n}_{L\sigma}$) must intersect with one segment connecting two neighboring midpoints of the edge of cell L , two midpoints are denoted by M_3 and M_4 , the cross point is denoted by O_2 . θ_{L_1} is the angle between LO_2 and LM_3 , and θ_{L_2} is the angle between LO_2 and LM_4 . Denote $\theta_L = \theta_{L_1} + \theta_{L_2}$. We define \mathbf{t}_{KM_i} ($i = 1, 2$) the unit vector along the direction from K to M_i and define \mathbf{t}_{LM_i} ($i = 3, 4$) the unit vector along the direction from L to M_i .

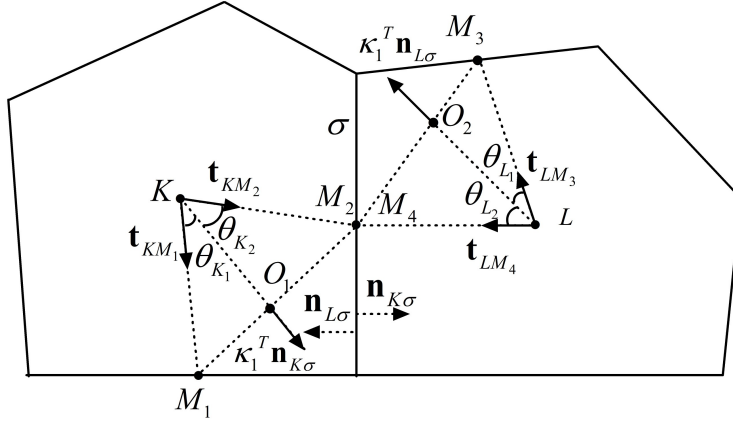


Fig. 3.1. The local stencil for local heat flux on interior cells.

3.2. The local heat flux

The discretization of unilateral normal heat flux is the same as that in [24] and the discretization on $\bar{\Omega}_1$ is the same as that on $\bar{\Omega}_2$. Hence we only overview the discretization of unilateral normal heat flux on $\bar{\Omega}_1$. Denote by $U = \{U_1, U_2\}$ the numerical solution of the DMP-preserving scheme on $\bar{\Omega}$, where U_1 is the solution on $\bar{\Omega}_1$ and U_2 is the solution on $\bar{\Omega}_2$.

Integrating Eq. (2.1) on cell $K \in \mathcal{J}_1$ yields

$$\sum_{\sigma \in \mathcal{E}_K} \mathcal{F}_{K,\sigma} = \int_K f(\mathbf{x}) d\mathbf{x},$$

where $\mathcal{F}_{K,\sigma}$ is the exact normal heat flux on edge σ and it can be written as

$$\mathcal{F}_{K,\sigma} = - \int_{\sigma} \nabla u_1(\mathbf{x}) \cdot \kappa_1^T(\mathbf{x}) \mathbf{n}_{K\sigma} dl.$$

Then we overview the discretization of unilateral normal heat flux. The discretization is divided into three cases, which are

- Case 1: on internal cells,
- Case 2: on interface,
- Case 3: on external boundary.

We demonstrate the construction process in Sections 3.2.1–3.2.3.

3.2.1. Case 1: The local heat flux on internal cells

The discretization of unilateral normal heat flux for internal cell $K \in \mathcal{J}_1$ can be found in Section 3.1.1 of [24]. The stencil of this case is plotted in Fig. 3.1. We just give the final expressions of numerical unilateral normal fluxes $F_1^{(1)}$ and $F_2^{(1)}$:

$$F_1^{(1)} = -|\kappa_1^T(K)\mathbf{n}_{K\sigma}||\sigma| \left(\frac{\sin\theta_{K_2}}{\sin\theta_K} \frac{1}{|KM_1|} \sum_{j=1}^{J_{M_1,n}} \omega_{M_1,j} (U_1(K_{M_1,j}) - U_1(K)) \right. \\ \left. + \frac{\sin\theta_{K_1}}{\sin\theta_K} \frac{1}{|KM_2|} \sum_{j=1}^{J_{M_2,n}} \omega_{M_2,j} (U_1(K_{M_2,j}) - U_1(K)) \right), \quad (3.1)$$

$$F_2^{(1)} = -|\kappa_1^T(L)\mathbf{n}_{L\sigma}||\sigma| \left(\frac{\sin\theta_{L_2}}{\sin\theta_L} \frac{1}{|LM_3|} \sum_{j=1}^{J_{M_3,n}} \omega_{M_3,j} (U_1(L_{M_3,j}) - U_1(L)) \right. \\ \left. + \frac{\sin\theta_{L_1}}{\sin\theta_L} \frac{1}{|LM_4|} \sum_{j=1}^{J_{M_4,n}} \omega_{M_4,j} (U_1(L_{M_4,j}) - U_1(L)) \right), \quad (3.2)$$

where $\omega_{M_i,j}$ ($i = 1, \dots, 4$) should be non-negative, its computation is proposed in [23].

3.2.2. Case 2: The local heat flux on the interface

The discretization of the unilateral normal heat flux for ghost cell $K \in \mathcal{J}_1^\Gamma$ can be found in Section 3.1.2 of [24]. There exists a cell $L \in \mathcal{J}_1$ such that $K \cap L = \sigma$, where σ is the common edge. A ray originating at the point K along the direction $\kappa_1^T \mathbf{n}_{K\sigma}$ must intersect with one point on the edge of cell L , denoted by K' . We suppose that K' is not located on the interface and plot the local stencil in Fig. 3.2.

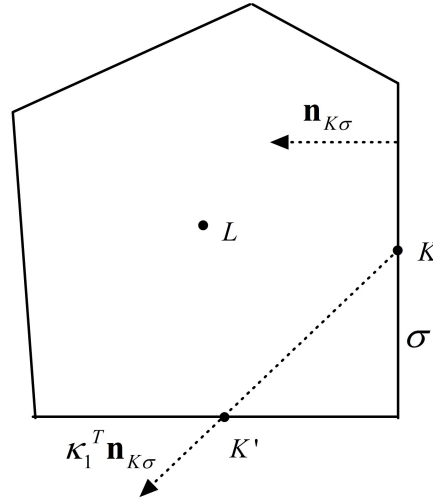


Fig. 3.2. The local stencil for local heat flux on interface Γ .

Similar to the derivation in Case 1, we get the unilateral normal heat flux

$$F_1^{(1)} = -|\kappa_1^T(K)\mathbf{n}_{K\sigma}||\sigma| \left(\frac{U_1(K') - U_1(K)}{|KK'|} \right).$$

The approximation of $U_1(K')$ is similar to that of $U_1(M_i)$ in [23]. $U_1(K')$ can be approximated by surrounding cell-centered unknowns with second order accuracy, i.e.,

$$U_1(K') \approx \sum_{j=1}^{J_{K',n}} \omega_{K',j} U_1(K_{K',j}),$$

where the coefficients $\omega_{K',j}$ are also required to be non-negative. This leads to

$$F_1^{(1)} = -|\kappa_1^T(K)\mathbf{n}_{K\sigma}||\sigma| \left(\sum_{j=1}^{J_{K',n}} \omega_{K',j} \frac{U_1(K_{K',j}) - U_1(K)}{|KK'|} \right). \quad (3.3)$$

The numerical unilateral normal flux $F_2^{(1)}$ is constructed in (3.2) for $L \in \mathcal{J}_1$.

3.2.3. Case 3: The local heat flux on the external boundary

The discretization of the unilateral normal flux for ghost cell $K \in \mathcal{J}_1^{out}$ can be found in Section 3.1.3 of [24]. There exists a cell $L \in \mathcal{J}_1$ such that $K \cap L = \sigma$, where σ is the common edge. A ray originating at the point K along the direction $\kappa_1^T \mathbf{n}_{K\sigma}$ must intersect with one point on edge LP_1 or LP_2 , denoted by O_1 . θ_{K_1} is the angle between KO_1 and KP_1 or KP_2 , and θ_{K_2} is the angle between KO_1 and KL . We show the local stencil in Fig. 3.3.

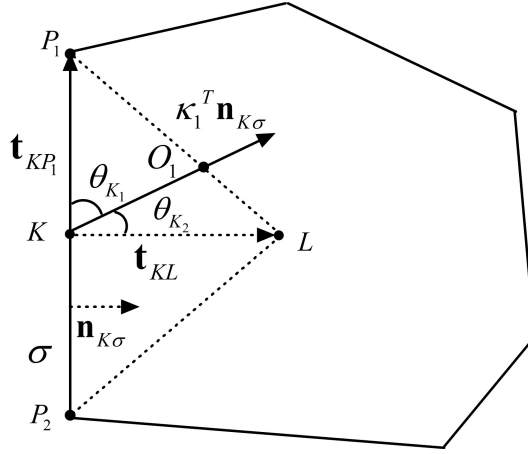


Fig. 3.3. The local stencil for local heat flux on external boundary.

The vector $\frac{\kappa_1^T(K)\mathbf{n}_{K\sigma}}{|\kappa_1^T(K)\mathbf{n}_{K\sigma}|}$ can be convexly decomposed by vector \mathbf{t}_{KP_1} (or \mathbf{t}_{KP_2}) and vector \mathbf{t}_{KL} , which implies that

$$\frac{\kappa_1^T(K)\mathbf{n}_{K\sigma}}{|\kappa_1^T(K)\mathbf{n}_{K\sigma}|} = \frac{\sin \theta_{K_2}}{\sin \theta_K} \mathbf{t}_{KP_1} + \frac{\sin \theta_{K_1}}{\sin \theta_K} \mathbf{t}_{KL}.$$

Then the discrete unilateral normal heat flux F_1^1 is defined as follows:

$$F_1^{(1)} = -|\kappa_1^T(K)\mathbf{n}_{K\sigma}||\sigma| \left(\frac{\sin \theta_{K_2}}{\sin \theta_K} \frac{U_1(P_1) - U_1(K)}{|KP_1|} + \frac{\sin \theta_{K_1}}{\sin \theta_K} \frac{U_1(L) - U_1(K)}{|KL|} \right).$$

The unilateral normal flux $F_2^{(1)}$ is constructed in (3.2) for $L \in \mathcal{J}_1$.

3.3. The conservative heat flux

In this section, we give the construction of conservative heat flux. The discrete unilateral normal heat fluxes can be written as

$$\begin{aligned} F_1^{(1)} &= \bar{F}'_1 + a_K^{(1)} (U_1(K) - U_1(L)), \\ F_2^{(1)} &= \bar{F}'_2 + a_L^{(1)} (U_1(L) - U_1(K)), \end{aligned}$$

where \bar{F}'_1 does not consist of the term $U_1(K) - U_1(L)$, \bar{F}'_2 does not consist of the term $U_1(L) - U_1(K)$. According to the construction of unilateral normal heat fluxes, we have $a_K^{(1)} \geq 0$ and $a_L^{(1)} \geq 0$.

Define

$$a^{(1)} = \min(a_K^{(1)}, a_L^{(1)}),$$

and rewrite the unilateral normal heat fluxes:

$$\begin{aligned} F_1^{(1)} &= \bar{F}_1^{(1)} + a^{(1)} (U_1(K) - U_1(L)), \\ F_2^{(1)} &= \bar{F}_2^{(1)} + a^{(1)} (U_1(L) - U_1(K)). \end{aligned}$$

According to the definition, we obtain $a^{(1)} \geq 0$.

Finally, we give the construction of conservative heat flux on $\bar{\Omega}_1$. For any edge $\sigma \in \mathcal{E}_1$, there exist cell $K \in \mathcal{J}_1 \cup \mathcal{J}_1^\Gamma$ and cell $L \in \mathcal{J}_1 \cup \mathcal{J}_1^\Gamma$ such that $K \cap L = \sigma$. The expressions of conservative heat fluxes are

$$\begin{aligned} F_{K,\sigma}^{(1)} &= a^{(1)} (U_1(K) - U_1(L)) + C_1^{(1)} \bar{F}_1^{(1)}, \\ F_{L,\sigma}^{(1)} &= a^{(1)} (U_1(L) - U_1(K)) + C_2^{(1)} \bar{F}_2^{(1)}, \end{aligned}$$

where $C_1^{(1)}$ and $C_2^{(1)}$ are nonlinear coefficients satisfying $C_1^{(1)} \geq 0$ and $C_2^{(1)} \geq 0$. The choice of $C_1^{(1)}$ and $C_2^{(1)}$ can be divided into two cases:

- (1) If $\bar{F}_1^{(1)} \bar{F}_2^{(1)} \geq 0$, we choose

$$C_1^{(1)} = C_2^{(1)} = 0.$$

- (2) If $\bar{F}_1^{(1)} \bar{F}_2^{(1)} < 0$, we choose

$$C_1^{(1)} = \frac{2|\bar{F}_2^{(1)}|}{|\bar{F}_1^{(1)}| + |\bar{F}_2^{(1)}|}, \quad C_2^{(1)} = \frac{2|\bar{F}_1^{(1)}|}{|\bar{F}_1^{(1)}| + |\bar{F}_2^{(1)}|}.$$

The construction of conservative numerical heat flux on $\bar{\Omega}_2$ is the same as that on $\bar{\Omega}_1$. For any $\sigma \in \mathcal{E}_2$, there exist $K \in \mathcal{J}_2 \cup \mathcal{J}_2^\Gamma$ and $L \in \mathcal{J}_2 \cup \mathcal{J}_2^\Gamma$ such that $K \cap L = \sigma$. Repeating the same process on $\bar{\Omega}_2$, the unilateral normal heat fluxes $F_1^{(2)}$, $F_2^{(2)}$, $a^{(2)}$, $\bar{F}_1^{(2)}$ and $\bar{F}_2^{(2)}$ are constructed similarly. Then we define the conservative heat fluxes as

$$\begin{aligned} F_{K,\sigma}^{(2)} &= a^{(2)} (U_2(K) - U_2(L)) + C_1^{(2)} \bar{F}_1^{(2)}, \\ F_{L,\sigma}^{(2)} &= a^{(2)} (U_2(L) - U_2(K)) + C_2^{(2)} \bar{F}_2^{(2)}, \end{aligned}$$

where $a^{(2)} \geq 0$, $C_1^{(2)}$ and $C_2^{(2)}$ are the nonlinear coefficients satisfying $C_1^{(2)} \geq 0$ and $C_2^{(2)} \geq 0$. The choice of $C_1^{(2)}$ and $C_2^{(2)}$ is similar to $C_1^{(1)}$ and $C_2^{(1)}$:

(1) If $\bar{F}_1^{(2)}\bar{F}_2^{(2)} \geq 0$, we choose

$$C_1^{(2)} = C_2^{(2)} = 0.$$

(2) If $\bar{F}_1^{(2)}\bar{F}_2^{(2)} < 0$, we choose

$$C_1^{(2)} = \frac{2|\bar{F}_2^{(2)}|}{|\bar{F}_1^{(2)}| + |\bar{F}_2^{(2)}|}, \quad C_2^{(2)} = \frac{2|\bar{F}_1^{(2)}|}{|\bar{F}_1^{(2)}| + |\bar{F}_2^{(2)}|}.$$

Remark 3.1. For $i = 1, 2$, if $a^{(i)} = 0$ and $C_1^{(i)} = C_2^{(i)} = 0$, we set $a^{(i)}$ to be a small constant 10^{-10} to avoid the singularity of the system.

3.4. The discretization on interface

The discretization on interface is the key to deal with the general case $\mu(\mathbf{x}) \geq 0$. We consider the general interface conditions:

$$u_2(\mathbf{x}) - u_1(\mathbf{x}) = \mu(\mathbf{x})\kappa_1(\mathbf{x})\nabla u_1(\mathbf{x}) \cdot \mathbf{n}_1, \quad \text{on } \Gamma, \quad (3.4)$$

$$\kappa_1(\mathbf{x})\nabla u_1(\mathbf{x}) \cdot \mathbf{n}_1 = -\kappa_2(\mathbf{x})\nabla u_2(\mathbf{x}) \cdot \mathbf{n}_2, \quad \text{on } \Gamma. \quad (3.5)$$

For any $\sigma \subset \Gamma$, there exist ghost cells $K_1 \in \mathcal{J}_1^\Gamma$ and $K_2 \in \mathcal{J}_2^\Gamma$ such that $K_1 = K_2 = \sigma$. Integrating equation (3.4) on K_1 yields

$$\int_\sigma u_1(\mathbf{x})dl + \int_\sigma \mu(\mathbf{x})\kappa_1(\mathbf{x})\nabla u_1(\mathbf{x}) \cdot \mathbf{n}_1 dl = \int_\sigma u_2(\mathbf{x})dl.$$

Hence we obtain the discretization of equation (3.4)

$$|\sigma|U_1(K_1) + \mu_{K_1}F_{K_1,\sigma}^{(1)} = |\sigma|U_2(K_2), \quad (3.6)$$

where $\mu_{K_1} = \mu(K_1)$ and $F_{K_1,\sigma}^{(1)}$ is defined in Section 3.3.

Integrating equation (3.5) on K_1 yields

$$\int_\sigma \kappa_1(\mathbf{x})\nabla u_1(\mathbf{x}) \cdot \mathbf{n}_1 dl + \int_\sigma \kappa_2(\mathbf{x})\nabla u_2(\mathbf{x}) \cdot \mathbf{n}_2 dl = 0.$$

Hence we obtain the discretization of equation (3.5)

$$F_{K_1,\sigma}^{(1)} + F_{K_2,\sigma}^{(2)} = 0, \quad (3.7)$$

which means the numerical normal heat flux is conservative for the general interface condition $\mu \geq 0$.

3.5. The finite volume scheme

Let $U = \{U_1, U_2\}$ be a N -dimensional numerical solution vector consisting of cell centered-unknowns. The DMP-preserving finite volume scheme for general interface problem (2.1)-(2.6)

with $\mu \geq 0$ is constructed in (3.8)-(3.13):

$$\sum_{\sigma_1 \in \mathcal{E}_{K_1}} F_{K_1, \sigma_1}^{(1)} = f_{K_1} m(K_1), \quad \forall K_1 \in \mathcal{J}_1, \quad (3.8)$$

$$\sum_{\sigma_2 \in \mathcal{E}_{K_2}} F_{K_2, \sigma_2}^{(2)} = f_{K_2} m(K_2), \quad \forall K_2 \in \mathcal{J}_2, \quad (3.9)$$

$$U_1(K_1) = g_{K_1}, \quad \forall K_1 \in \mathcal{J}_1^{out}, \quad (3.10)$$

$$U_2(K_2) = g_{K_2}, \quad \forall K_2 \in \mathcal{J}_2^{out}, \quad (3.11)$$

where $m(K_1)$ denotes the area of cell K_1 , f_{K_1} and g_{K_1} denote the values of $f(\mathbf{x})$ and $g(\mathbf{x})$ at cell center K_1 .

For any edge $\sigma \in \Gamma$, there exist ghost cells $K_1 \in \mathcal{J}_1^\Gamma$ and $K_2 \in \mathcal{J}_2^\Gamma$ such that $K_1 = K_2 = \sigma$. The discretization on interface is

$$|\sigma|U_1(K_1) + \mu_{K_1} F_{K_1, \sigma}^{(1)} = |\sigma|U_2(K_2), \quad \forall \sigma \in \Gamma, \quad (3.12)$$

$$F_{K_1, \sigma}^{(1)} + F_{K_2, \sigma}^{(2)} = 0, \quad \forall \sigma \in \Gamma. \quad (3.13)$$

The nonlinear system of finite volume scheme (3.8)-(3.13) is denoted by

$$A(U)U = F(f, g), \quad (3.14)$$

where $A(U)$ is the corresponding $N \times N$ dimensional nonlinear coefficient matrix and $F(f, g)$ is a N -dimensional right-hand-side vector associated with source term $f(\mathbf{x})$ and Dirichlet boundary condition $g(\mathbf{x})$.

We demonstrate the finite volume scheme (3.15)-(3.20) proposed in [24] for imperfect interface problem with $\mu > 0$:

$$\sum_{\sigma_1 \in \mathcal{E}_{K_1}} F_{K_1, \sigma_1}^{(1)} = f_{K_1} m(K_1), \quad \forall K_1 \in \mathcal{J}_1, \quad (3.15)$$

$$\sum_{\sigma_2 \in \mathcal{E}_{K_2}} F_{K_2, \sigma_2}^{(2)} = f_{K_2} m(K_2), \quad \forall K_2 \in \mathcal{J}_2, \quad (3.16)$$

$$U_1(K_1) = g_{K_1}, \quad \forall K_1 \in \mathcal{J}_1^{out}, \quad (3.17)$$

$$U_2(K_2) = g_{K_2}, \quad \forall K_2 \in \mathcal{J}_2^{out}. \quad (3.18)$$

For any edge $\sigma \in \Gamma$, there exist ghost cells $K_1 \in \mathcal{J}_1^\Gamma$ and $K_2 \in \mathcal{J}_2^\Gamma$ such that $K_1 = K_2 = \sigma$. The discretization in [24] on the interface is

$$|\sigma|U_1(K_1) + \mu_{K_1} F_{K_1, \sigma}^{(1)} = |\sigma|U_2(K_2), \quad \forall \sigma \in \Gamma, \quad (3.19)$$

$$|\sigma|U_2(K_2) + \mu_{K_2} F_{K_2, \sigma}^{(2)} = |\sigma|U_1(K_1), \quad \forall \sigma \in \Gamma. \quad (3.20)$$

When $\mu \equiv 0$, (3.19) and (3.20) are exactly the same, hence the two lines corresponding to (3.19) and (3.20) are the same in the matrix. In this case, the matrix in [24] is singular. This is the reason why the scheme in [24] cannot handle zero interfacial coefficient.

Remark 3.2. The difference between the unified scheme proposed in this paper and the finite volume scheme in [24] is the discretization on the interface. The discretization of Eq. (3.4) in [24] is the same as (3.6), but the discretization of Eq. (3.5) is different. When the interfacial

coefficient degenerates to somewhere, the nonlinear system of our scheme is not singular, but the nonlinear system in [24] is singular because of the discretization on the interface (3.19) and (3.20). Eqs. (3.19)-(3.20) are linearly dependent in the matrix when $\mu = 0$. This is the reason why the scheme proposed in this paper can deal with the general interfacial coefficient $\mu \geq 0$, but the scheme in [24] can not.

We employ Picard iteration to solve the nonlinear system (3.14). In the algorithm, we choose parameters ε_{non} and \max_{it} , which represent the nonlinear iteration threshold and maximum number of nonlinear iteration, respectively. The algorithm is summarized as follows:

Algorithm 3.1. Picard iteration

- 1: Choose a initial vector U^0 ;
- 2: **while** $\|A(U^k)U^k - F\| > \varepsilon_{non}\|A(U^0)U^0 - F\|$ and $k \leq \max_{it}$ **do**
- 3: Solve the linear system $A(U^k)U^{k+1} = F$;
- 4: Let $k = k + 1$;
- 5: **end while**

Remark 3.3. The second difference between the scheme proposed in this paper and the finite volume scheme in [24] is the way to solve the corresponding nonlinear finite volume scheme. Picard iteration is employed to solve the nonlinear scheme in this paper. The domain decomposition method called Robin-Robin is employed to solve the nonlinear scheme in [24].

4. The DMP-preserving Property and Existence of Solution

In this section, the DMP-preserving property of the finite volume scheme (3.8)-(3.13) is proved, and the existence of solution is also proved. Moreover, when the interfacial coefficients tend to zero, we prove that the numerical solutions of scheme (3.8)-(3.13) has a subsequence converging to the numerical solution of the perfect interface problem.

For the finite volume scheme (3.8)-(3.13), the DMP is as follows:

Theorem 4.1. Denote $U_{\min} = \min_{K \in \mathcal{J} \cup \mathcal{J}^{out} \cup \mathcal{J}^\Gamma} U(K)$ and $U_{\max} = \max_{K \in \mathcal{J} \cup \mathcal{J}^{out} \cup \mathcal{J}^\Gamma} U(K)$, then it holds that:

- (i) assume that $f(\mathbf{x}) \geq 0$, if U is not a constant on $\bar{\Omega}$, then U_{\min} can only be attained on $\partial\Omega$;
- (ii) assume that $f(\mathbf{x}) \leq 0$, if U is not a constant on $\bar{\Omega}$, then U_{\max} can only be attained on $\partial\Omega$;
- (iii) assume that $f(\mathbf{x}) = 0$, if U is not a constant on $\bar{\Omega}$, then U_{\max} and U_{\min} can only be attained on $\partial\Omega$.

Proof. We follow the idea of the proof of Theorem 2 in [24] to prove the case $f(\mathbf{x}) \geq 0$. The proofs of $f(\mathbf{x}) \leq 0$ and $f(\mathbf{x}) = 0$ are similar, which are omitted.

For any cell $K_1 \in \mathcal{J}_1 \cup \mathcal{J}_1^\Gamma$, $\sigma_1 \in \mathcal{E}_{K_1}$ and cell $K_2 \in \mathcal{J}_2 \cup \mathcal{J}_2^\Gamma$, $\sigma_2 \in \mathcal{E}_{K_2}$, the expressions of

conservative heat flux $F_{K_1, \sigma_1}^{(1)}$ and $F_{K_2, \sigma_2}^{(2)}$ are as follows:

$$F_{K_1, \sigma_1}^{(1)} = - \sum_{j=1}^{N_{K_1, \sigma_1}^{(1)}} A_{K_1, \sigma_1, j}^{(1)} (U_1(L_{K_1, j}) - U_1(K_1)), \quad (4.1)$$

$$F_{K_2, \sigma_2}^{(2)} = - \sum_{j=1}^{N_{K_2, \sigma_2}^{(2)}} A_{K_2, \sigma_2, j}^{(2)} (U_2(L_{K_2, j}) - U_2(K_2)), \quad (4.2)$$

where $N_{K_1, \sigma_1}^{(1)}$ is the number of cells associated with cell K_1 in the $F_{K_1, \sigma_1}^{(1)}$, $N_{K_2, \sigma_2}^{(2)}$ is defined similarly. There hold $A_{K_1, \sigma_1, j}^{(1)} \geq 0$ and $A_{K_2, \sigma_2, j}^{(2)} \geq 0$ according to the construction of the conservative heat flux.

Substituting the expressions of conservative heat fluxes $F_{K_1, \sigma_1}^{(1)}$ and $F_{K_2, \sigma_2}^{(2)}$ into (3.8)-(3.13), then the finite volume scheme can be rewritten as

$$- \sum_{j=1}^{N_{K_1}^{(1)}} A_{K_1, j}^{(1)} (U_1(L_{K_1, j}) - U_1(K_1)) = f_{K_1} m(K_1), \quad \forall K_1 \in \mathcal{J}_1, \quad (4.3)$$

$$- \sum_{j=1}^{N_{K_2}^{(2)}} A_{K_2, j}^{(2)} (U_2(L_{K_2, j}) - U_2(K_2)) = f_{K_2} m(K_2), \quad \forall K_2 \in \mathcal{J}_2, \quad (4.4)$$

and for any $\sigma \subset \Gamma$, there exist ghost cells $K_1 \in \mathcal{J}_1^\Gamma$ and $K_2 \in \mathcal{J}_2^\Gamma$ such that $K_1 = K_2 = \sigma$. The discretization on the interface is

$$|\sigma| U_1(K_1) - \mu_{K_1} \sum_{j=1}^{N_{K_1}^{(1)}} A_{K_1, j}^{(1)} (U_1(L_{K_1, j}) - U_1(K_1)) = |\sigma| U_2(K_2), \quad \forall \sigma \subset \Gamma, \quad (4.5)$$

$$- \mu_{K_1} \sum_{j=1}^{N_{K_1}^{(1)}} A_{K_1, j}^{(1)} (U_1(L_{K_1, j}) - U_1(K_1)) - \mu_{K_2} \sum_{j=1}^{N_{K_2}^{(2)}} A_{K_2, j}^{(2)} (U_2(L_{K_2, j}) - U_2(K_2)) = 0, \quad (4.6)$$

$$\forall \sigma \subset \Gamma,$$

where $A_{K_1, j}^{(1)}$ is the sum of $A_{K_1, \sigma_1, j}^{(1)}$, $N_{K_1}^{(1)}$ is the number of cells associated with cell K_1 in the scheme, $A_{K_2, j}^{(2)}$ and $N_{K_2}^{(2)}$ are defined similarly. There hold $A_{K_1, j}^{(1)} \geq 0$ and $A_{K_2, j}^{(2)} \geq 0$.

Assuming that U reaches its minimum on Ω , then the conclusion that U is a constant on $\bar{\Omega}$ need to be proved. According to the assumption, we denote cell $K_0 \in \mathcal{J} \cup \mathcal{J}^\Gamma$ such that U reaches its minimum on K_0 . The location of K_0 can be divided into four cases, which are $K_0 \in \mathcal{J}_1$, $K_0 \in \mathcal{J}_2$, $K_0 \in \mathcal{J}_1^\Gamma$ and $K_0 \in \mathcal{J}_2^\Gamma$, respectively. For the first three cases, the proof is same as the proof of Theorem 2 in [24]. Hence we only consider the last case.

In this case, U attain its minimum on $K_0 \in \mathcal{J}_2^\Gamma$. It holds $U_2(L_{K_0, j}) - U_2(K_0) \geq 0$ for all $L_{K_0, j} \in \mathcal{J}_2 \cup \mathcal{J}_2^\Gamma$, which implies that

$$- \sum_{j=1}^{N_{K_0}^{(2)}} A_{K_0, j}^{(2)} (U_2(L_{K_0, j}) - U_2(K_0)) \leq 0. \quad (4.7)$$

Denote by ghost cell $K_1 \in \mathcal{J}_1^\Gamma$ such that $K_1 = K_0 = \sigma \subset \Gamma$. Substituting (4.7) into (4.6), then it holds that

$$-\sum_{j=1}^{N_{K_1}^{(1)}} A_{K_1,j}^{(1)} (U_1(L_{K_1,j}) - U_1(K_1)) \geq 0. \quad (4.8)$$

Substituting (4.8) into (4.5), then it holds that

$$U_1(K_1) \leq U_2(K_0) = U_{\min}, \quad (4.9)$$

which implies that U reaches its minimum on $K_1 \in \mathcal{J}_1^\Gamma$. According to the conclusion of Case 2, U is a constant on $\bar{\Omega}$. \square

We also remark that the solution of the finite volume scheme (3.8)-(3.13) exists for $f(\mathbf{x}) \equiv 0$. The proof is analogous to that in Theorem 3 in [24] and is left to the reader.

Theorem 4.2. *Suppose $f(\mathbf{x}) \equiv 0$, then the nonlinear finite volume scheme (3.8)-(3.13) has at least one solution $U = \{U(K)\}$ for any general interfacial coefficient $\mu(\mathbf{x}) \geq 0$.*

It should be noticed that our scheme (3.8)-(3.13) is indeed the scheme for perfect interface problem when $\mu(\mathbf{x}) \equiv 0$. The scheme for perfect interface problem is described as follows:

$$\sum_{\sigma_1 \in \mathcal{E}_{K_1}} F_{K_1,\sigma_1}^{(1)} = f_{K_1} m(K_1), \quad \forall K_1 \in \mathcal{J}_1, \quad (4.10)$$

$$\sum_{\sigma_2 \in \mathcal{E}_{K_2}} F_{K_2,\sigma_2}^{(2)} = f_{K_2} m(K_2), \quad \forall K_2 \in \mathcal{J}_2, \quad (4.11)$$

$$U_1(K_1) = g_{K_1}, \quad \forall K_1 \in \mathcal{J}_1^{out}, \quad (4.12)$$

$$U_2(K_2) = g_{K_2}, \quad \forall K_2 \in \mathcal{J}_2^{out}. \quad (4.13)$$

For any edge $\sigma \subset \Gamma$, there exist ghost cells $K_1 \in \mathcal{J}_1^\Gamma$ and $K_2 \in \mathcal{J}_2^\Gamma$ such that $K_1 = K_2 = \sigma$. The discretization on interface for perfect interface problem is

$$U_1(K_1) = U_2(K_2), \quad \forall \sigma \subset \Gamma, \quad (4.14)$$

$$F_{K_1,\sigma}^{(1)} + F_{K_2,\sigma}^{(2)} = 0, \quad \forall \sigma \subset \Gamma. \quad (4.15)$$

We conclude this section by revealing that the preliminary convergence relationship between numerical solutions of the interface problem with general interfacial coefficient and the perfect interface problem. With the help of Theorem 4.2, the following theorem and corollary hold when $f(\mathbf{x}) \equiv 0$. The proofs of Theorem 4.3 and Corollary 4.1 are also analogous to that in Theorem 4 and Corollary 1 in [24], which are left to the reader.

Theorem 4.3. *Suppose $f(\mathbf{x}) \equiv 0$ and $\{\mu_i(\mathbf{x})\}_{i=1}^\infty$ is a sequence of function tending to zero uniformly when $i \rightarrow \infty$. For any $\mu_i(\mathbf{x}) \geq 0$, we denote U^{μ_i} the solution of finite volume scheme (3.8)-(3.13) for interface problem with general interfacial coefficient. When $i \rightarrow \infty$, there exists a subsequence of $\{U^{\mu_i}\}_{i=1}^\infty$ converging to the solution of finite volume scheme (4.10)-(4.15) for the perfect interface problem.*

Corollary 4.1. *Suppose the solution of scheme (4.10)-(4.15) for perfect interface problem is unique, then the whole sequence $\{U^{\mu_i}\}_{i=1}^\infty$ in Theorem 4.3 converges to the numerical solution of perfect interface problem when $i \rightarrow \infty$.*

5. Numerical Experiments

In this section, numerical examples are presented to show the accuracy and the DMP-preserving property of our scheme. The DMP-preserving finite volume scheme in [24], which is only designed for positive interfacial coefficient, is compared with our scheme. We compare the accuracy and nonlinear iteration number of the two schemes under $\mu \rightarrow 0$ and $\mu \geq 0$.

In the numerical experiments, we observe that the nonlinear iteration numbers of the scheme in [24] increase rapidly as μ tending to zero. The computation cost is too large when μ is very small, although second order accuracy is obtained. While the iteration numbers of our scheme in this paper do not increase as μ tending to 0, and second order accuracy is also obtained. We also observe that the scheme in [24] loses accuracy for interface problem when the interfacial coefficient $\mu(\mathbf{x})$ degenerates to zero somewhere. The numerical results reveal that the unified scheme is efficient for $\mu \geq 0$ and is more robust than the finite volume scheme in [24].

We define

$$\mathcal{E}_2^u = \left[\sum_{K \in \mathcal{J}_1 \cup \mathcal{J}_2} (U(K) - u(K))^2 m(K) \right]^{1/2}$$

to evaluate the approximate error of solution, and

$$\mathcal{E}_2^F = \left[\sum_{\sigma \in \mathcal{E}_1} \left(F_{K,\sigma}^{(1)} - \mathcal{F}_{K,\sigma}^{(1)} \right)^2 + \sum_{\sigma \in \mathcal{E}_2} \left(F_{K,\sigma}^{(2)} - \mathcal{F}_{K,\sigma}^{(2)} \right)^2 \right]^{1/2}$$

to evaluate the approximate error of flux. In all the examples, we set the initial vector $U^0 = 1$, nonlinear iteration threshold $\varepsilon_{non} = 10^{-8}$ and maximum number of nonlinear iteration $\max_{it} = 5000$.

5.1. Example 1: comparison under different interfacial coefficients

In the first example, we compare the performance of our scheme and the DMP-preserving scheme in [24] under different interfacial coefficients. We list the accuracy and nonlinear iteration numbers of the two schemes when μ tends to zero.

Consider the square domain that $\Omega = (0, 1) \times (0, 1) = \Omega_1 \cup \Omega_2 \cup \Gamma$, where $\Omega_1 = (0, 0.5) \times (0, 1)$ and $\Omega_2 = (0.5, 1) \times (0, 1)$. The interface $\Gamma = \{(x, y) | x = 0.5\}$, which is presented in Fig. 5.1. We take exact solution as

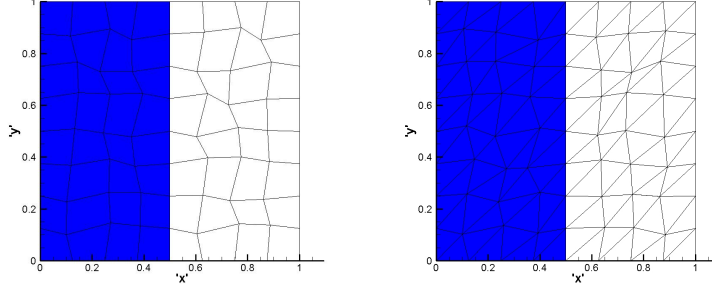
$$u(x, y) = \begin{cases} x + \sin(y), & \text{in } \Omega_1, \\ tx + \sin(ty), & \text{in } \Omega_2, \end{cases}$$

and take $\kappa_1 = tI$, $\kappa_2 = I$, $\mu(y) = \frac{1}{t}(0.5(t-1) + \sin(ty) - \sin y)$, where t is a positive adjustable parameter. $f(x, y)$ can be calculated accordingly. We can easily see that μ tends to zero uniformly when t tends to 1 and the problem degenerates to perfect interface problem when $t = 1$. Denote $\mu_{\min} = \min_{0 \leq y \leq 1} \mu(y)$ and $\mu_{\max} = \max_{0 \leq y \leq 1} \mu(y)$. In the numerical experiments, we take $t = 2$, $t = 1.01$, $t = 1.001$, and $t = 1$, separately. The maxima and minima of μ for different t are shown in Table 5.1.

First, we compare our scheme with the scheme in [24] on random quadrilateral meshes for this problem. The random quadrilateral meshes are generated by the uniform rectangular meshes whose vertex coordinates are perturbed randomly in $[-\sigma h/2, \sigma h/2] \times [-\sigma h/2, \sigma h/2]$

Table 5.1: The maxima and minima of μ for different t .

t	2	1.01	1.001	1
μ_{\max}	4.35E-01	1.05E-02	1.06E-03	0
μ_{\min}	2.50E-01	4.95E-03	5.00E-04	0



(a) The random quadrilateral meshes. (b) The random triangular meshes.

Fig. 5.1. The random meshes of Ω .

Table 5.2: Numerical results of our scheme for Example 1 on the random quadrilateral meshes.

N_c		64	256	1024	4048	16384
$t=2$	\mathcal{E}_2^u	1.95E-03	4.95E-04	1.45E-04	3.02E-05	7.65E-06
	order		1.98	1.77	2.26	1.98
	\mathcal{E}_2^F	2.38E-02	7.10E-03	3.14E-03	1.39E-03	7.10E-04
	order		1.75	1.18	1.18	0.97
	non_{it}	18	18	20	20	20
$t=1.01$	\mathcal{E}_2^u	6.49E-04	1.49E-04	4.15E-05	1.03E-05	2.60E-06
	order		2.12	1.84	2.01	1.99
	\mathcal{E}_2^F	4.57E-03	1.53E-03	6.92E-04	3.13E-04	1.57E-04
	order		1.58	1.14	1.14	1.00
	non_{it}	20	18	19	19	18
$t=1.001$	\mathcal{E}_2^u	6.41E-04	1.47E-04	4.10E-05	1.01E-05	2.58E-06
	order		2.12	1.84	2.02	1.97
	\mathcal{E}_2^F	4.50E-03	1.51E-03	6.83E-04	3.07E-04	1.55E-04
	order		1.58	1.14	1.15	0.99
	non_{it}	20	18	19	19	18
$t=1$	\mathcal{E}_2^u	6.41E-04	1.47E-04	4.09E-05	1.01E-05	2.58E-06
	order		2.12	1.85	2.02	1.97
	\mathcal{E}_2^F	4.49E-03	1.50E-03	6.82E-04	3.07E-04	1.54E-04
	order		1.58	1.14	1.15	1.00
	non_{it}	20	18	19	19	18

and h denotes the mesh size of uniform meshes. The distortion is taken to be $\sigma = 0.4$ and the meshes are displayed in Fig. 5.1 (a). We define N_c the number of cells in Ω . The errors and nonlinear iteration numbers of our scheme and the scheme in [24] are listed in Table 5.2 and Table 5.3 for different t , respectively.

When $t > 1$, we observe from Table 5.2 and Table 5.3 that the errors of the two schemes are almost the same and both two schemes can obtain second order convergence for solution error

Table 5.3: Numerical results of the scheme in [24] for Example 1 on the random quadrilateral meshes.

N_c		64	256	1024	4048	16384
$t=2$	\mathcal{E}_2^u	1.95E-03	4.95E-04	1.45E-04	3.02E-05	7.65E-06
	order		1.98	1.77	2.26	1.98
	\mathcal{E}_2^F	2.38E-02	7.10E-03	3.14E-03	1.39E-03	7.10E-04
	order		1.75	1.18	1.18	0.97
	non_{it}	11	11	11	12	12
$t=1.01$	\mathcal{E}_2^u	6.49E-04	1.49E-04	4.15E-05	1.03E-05	2.60E-06
	order		2.12	1.84	2.01	1.99
	\mathcal{E}_2^F	4.57E-03	1.53E-03	6.92E-04	3.13E-04	1.57E-04
	order		1.58	1.14	1.14	1.00
	non_{it}	268	267	274	283	294
$t=1.001$	\mathcal{E}_2^u	6.42E-04	1.47E-04	4.10E-05	1.02E-05	2.58E-06
	order		2.13	1.84	2.01	1.98
	\mathcal{E}_2^F	4.50E-03	1.51E-03	6.83E-04	3.07E-04	1.55E-04
	order		1.58	1.14	1.15	0.99
	non_{it}	2233	2237	2308	2407	2517
$t=1$	\mathcal{E}_2^u	7.16E-02	8.00E-02	8.38E-02	8.51E-02	8.54E-02
	order		-0.16	-0.07	-0.02	-0.01
	\mathcal{E}_2^F	8.27E-01	9.98E-01	1.16E+00	1.30E+00	1.42E+00
	order		-0.27	-0.22	-0.16	-0.13
	non_{it}	2	2	2	2	2

Table 5.4: Numerical results of our scheme for Example 1 on the random triangular meshes.

N_c		128	512	2048	8096	32768
$t=2$	\mathcal{E}_2^u	1.59E-03	4.65E-04	1.17E-04	3.34E-05	8.17E-06
	order		1.77	1.99	1.81	2.03
	\mathcal{E}_2^F	3.83E-02	9.51E-03	4.38E-03	2.00E-03	9.02E-04
	order		2.01	1.12	1.13	1.15
	non_{it}	40	41	46	43	46
$t=1.01$	\mathcal{E}_2^u	2.31E-04	5.09E-05	1.32E-05	3.11E-06	7.82E-07
	order		2.18	1.95	2.09	1.99
	\mathcal{E}_2^F	6.05E-03	1.65E-03	8.46E-04	3.99E-04	1.97E-04
	order		1.87	0.96	1.08	1.02
	non_{it}	39	39	43	42	42
$t=1.001$	\mathcal{E}_2^u	2.28E-04	5.00E-05	1.30E-05	3.08E-06	7.76E-07
	order		2.19	1.94	2.08	1.99
	\mathcal{E}_2^F	5.93E-03	1.63E-03	8.32E-04	3.93E-04	1.94E-04
	order		1.86	0.97	1.08	1.02
	non_{it}	39	39	43	42	43
$t=1$	\mathcal{E}_2^u	2.27E-04	4.99E-05	1.30E-05	3.08E-06	7.74E-07
	order		2.19	1.94	2.08	1.99
	\mathcal{E}_2^F	5.92E-03	1.63E-03	8.29E-04	3.93E-04	1.94E-04
	order		1.86	0.98	1.08	1.02
	non_{it}	39	39	43	42	43

and first order convergence for flux error. However, the nonlinear iteration numbers of the two schemes are remarkable different. The nonlinear iteration numbers of the scheme in [24] increase rapidly as t tending to 1. Meanwhile, the nonlinear iteration numbers of our scheme almost do

Table 5.5: Numerical results of the scheme in [24] for Example 1 on the random triangular meshes.

N_c		128	512	2048	8096	32768
$t=2$	\mathcal{E}_2^u	1.59E-03	4.65E-04	1.17E-04	3.34E-05	8.16E-06
	order		1.77	1.99	1.81	2.03
	\mathcal{E}_2^F	3.83E-02	9.51E-03	4.38E-03	2.00E-03	9.02E-04
	order		2.01	1.12	1.13	1.15
	non_{it}	11	11	11	12	12
$t=1.01$	\mathcal{E}_2^u	2.31E-04	5.09E-05	1.32E-05	3.11E-06	7.82E-07
	order		2.18	1.95	2.09	1.99
	\mathcal{E}_2^F	6.05E-03	1.65E-03	8.46E-04	3.99E-04	1.97E-04
	order		1.87	0.96	1.08	1.02
	non_{it}	263	268	278	289	299
$t=1.001$	\mathcal{E}_2^u	2.28E-04	5.00E-05	1.30E-05	3.08E-06	7.76E-07
	order		2.19	1.94	2.08	1.99
	\mathcal{E}_2^F	5.93E-03	1.63E-03	8.32E-04	3.93E-04	1.94E-04
	order		1.86	0.97	1.08	1.02
	non_{it}	2191	2249	2349	2458	2562
$t=1$	\mathcal{E}_2^u	7.91E-02	8.35E-02	8.48E-02	8.54E-02	8.56E-02
	order		-0.08	-0.02	-0.01	-0.00
	\mathcal{E}_2^F	1.29E+00	1.52E+00	1.73E+00	1.91E+00	2.07E+00
	order		-0.24	-0.19	-0.14	-0.12
	non_{it}	2	2	2	2	2

not change as t tending to 1. When $t = 1$, we observe that the errors of the scheme [24] do not decrease when the meshes are refined. This verifies that the scheme in [24] is not valid for $\mu = 0$. Our scheme can still keep second order accuracy and the nonlinear iteration numbers do not remarkably increase for $\mu \geq 0$.

Then we compare our scheme with the scheme in [24] on random triangular meshes. The random triangular meshes are generated by the uniform triangular meshes whose vertex coordinates are perturbed randomly in $[-\sigma h/2, \sigma h/2] \times [-\sigma h/2, \sigma h/2]$, which the distortion $\sigma = 0.4$ and the meshes are displayed in Fig. 5.1 (b). The errors and nonlinear iteration numbers of our scheme and the scheme in [24] are listed in Table 5.4 and Table 5.5, respectively.

From Table 5.4 and Table 5.5, we observe that the performance of the two schemes on random triangular meshes is similar to that on random quadrilateral meshes. The nonlinear iteration numbers of the scheme in [24] increase rapidly as t tending to 1, and the errors of scheme in [24] do not decrease when the meshes are refined when $t = 1$. We notice that when $\mu \equiv 0$, the iteration numbers are always 2 in Robin-Robin iteration [24]. The algorithm of Robin-Robin iteration is presented in algorithm 1 of [24]. Meanwhile, our scheme can keep second order accuracy and the nonlinear iteration numbers do not rapidly increase for all $\mu \geq 0$. The iteration number of [24] is 140 times of the proposed scheme on average when $t = 1.001$ on random quadrilateral meshes. The numerical results show that our scheme is more robust than the scheme in [24]. The nonlinear finite volume scheme in [24] tends to be singular when the interfacial coefficients tend to zero, which may result in the rapid increase of the nonlinear iteration numbers. Compared to [24], the proposed scheme does not tend to singular when μ tends to zero and is nonsingular when $\mu = 0$, thus the nonlinear iteration numbers do not increase when the interfacial coefficients tend to zero.

5.2. Example 2: comparison under non-negative interfacial coefficient

In the previous example, we compared the performance of the two schemes for $\mu > 0$ and $\mu \equiv 0$. In this example, we will further compare the errors and iteration numbers of the two schemes for $\mu \geq 0$.

We take the same domain as that in Example 1 and take the exact solution

$$u(x, y) = \begin{cases} u_1(x, y), & \text{in } \Omega_1, \\ u_2(x, y), & \text{in } \Omega_2, \end{cases}$$

where

$$u_1(x, y) = x + (y - 0.5)^3, \quad u_2(x, y) = \begin{cases} 2x + (y - 0.5)^3, & \text{if } y > 0.5, \\ 2x, & \text{if } y \leq 0.5. \end{cases}$$

The diffusion coefficients are taken as $\kappa_1 = 2I$ and $\kappa_2 = I$. The interfacial coefficient μ is calculated as follows

$$\mu(x, y) = \begin{cases} 0, & y > 0.5, \\ 0.5(0.5 - y)^3, & y \leq 0.5. \end{cases}$$

and f can be calculated accordingly.

Table 5.6: Comparison of our scheme and the scheme in [24] for Example 2 on the random quadrilateral meshes.

N_c		64	256	1024	4048	16384
Our scheme	\mathcal{E}_2^u	2.37E-03	5.86E-04	1.51E-04	3.77E-05	9.57E-06
	order		2.02	1.96	2.00	1.98
	\mathcal{E}_2^F	3.29E-02	9.25E-03	3.78E-03	1.75E-03	7.98E-04
	order		1.83	1.29	1.11	1.13
	non_{it}	20	19	19	19	18
The scheme in [24]	\mathcal{E}_2^u	8.38E-03	8.23E-03	8.57E-03	8.81E-03	8.91E-03
	order		0.03	-0.06	-0.04	-0.02
	\mathcal{E}_2^F	1.75E-01	2.24E-01	2.97E-01	3.54E-01	3.91E-01
	order		-0.36	-0.41	-0.25	-0.14
	non_{it}	2768	5000	5000	5000	5000

Table 5.7: Comparison of our scheme and the scheme in [24] for Example 2 on the random triangular meshes.

N_c		128	512	2048	8096	32768
Our scheme	\mathcal{E}_2^u	7.83E-04	1.77E-04	4.51E-05	1.22E-05	3.10E-06
	order		2.15	1.97	1.89	1.98
	\mathcal{E}_2^F	3.06E-02	8.86E-03	3.89E-03	1.97E-03	9.74E-04
	order		1.79	1.19	0.98	1.02
	non_{it}	39	41	43	44	44
The scheme in [24]	\mathcal{E}_2^u	7.63E-03	8.30E-03	8.71E-03	8.85E-03	8.94E-03
	order		-0.12	-0.07	-0.02	-0.01
	\mathcal{E}_2^F	2.98E-01	3.98E-01	4.85E-01	5.49E-01	6.11E-01
	order		-0.42	-0.29	-0.18	-0.15
	non_{it}	2485	5000	5000	5000	5000

We compare the two schemes on random quadrilateral meshes and triangular meshes, and the numerical results are listed in Table 5.6 and Table 5.7, respectively. From Table 5.6 and Table 5.7 we observe that nonlinear iteration of the scheme in [24] does not converge and the scheme loses accuracy. Our scheme obtains second order accuracy for solution and the iteration numbers are stable for different meshes. The numerical results verify that our scheme is robust for $\mu \geq 0$, while the scheme in [24] is only valid for $\mu > 0$.

5.3. Example 3: accuracy for coefficients with large difference

In this example, we test the accuracy of our scheme when the diffusion coefficients differ greatly in the two subdomains. Take the subdomains Ω_1 and Ω_2 as half-circle regions

$$\Omega_1 = B\left(O_1, \frac{1}{2}\right) \cap \left\{(x, y) : x \leq \frac{1}{2}\right\}, \text{ where } O_1 = \left(\frac{1}{2}, \frac{1}{2}\right),$$

$$\Omega_2 = B(O_2, 1) \cap \left\{(x, y) : x \geq \frac{1}{2}\right\}, \text{ where } O_2 = \left(\frac{1 + \sqrt{3}}{2}, \frac{1}{2}\right),$$

where $B((x_0, y_0), r) := \{(x, y) : (x - x_0)^2 + (y - y_0)^2 \leq r^2\}$. The coefficients are selected as follows

$$\kappa_1 = 100 \begin{pmatrix} x^2 + y^2 + 1 & xy \\ -xy & x^2 + y^2 + 2 \end{pmatrix}, \quad \kappa_2 = \begin{pmatrix} x^2 + y^2 + 1 & xy \\ -xy & x^2 + y^2 + 2 \end{pmatrix}.$$

We consider the exact solution

$$u(x, y) = \begin{cases} xy^2 + 2x + 2, & \text{in } \Omega_1, \\ 100(xy^2 + 2x + 2), & \text{in } \Omega_2, \end{cases}$$

and the interfacial coefficient

$$\mu(x, y) = \frac{99(xy^2 + 2x + 2)}{100((x^2 + y^2 + 1)y^2 + 2x^2y^2)}.$$

Similarly, f can be calculated accordingly.

We test the problem on random triangular meshes. The initial meshes are displayed in Fig. 5.4, where the number of cell is 288. Then we refine the meshes four times to test the accuracy of the two schemes. The numerical result is listed in Table 5.8, in which second order convergence for solution and first order convergence for flux are obtained. Since the scale of exact solution and the exact flux are about 10^3 , the errors on coarse meshes are relatively large. The errors and iteration numbers show that our scheme is effective for the problem of coefficients with large difference.

Table 5.8: Numerical results for Example 3 on the random triangular meshes.

N_c	288	1152	4608	18432	73728
\mathcal{E}_2^u	1.03E+00	3.75E-01	9.32E-02	1.85E-02	4.51E-03
order		1.46	2.01	2.33	2.04
\mathcal{E}_2^F	6.71E+01	2.92E+01	1.31E+01	6.91E+00	3.30E+00
order		1.20	1.16	0.92	1.07
non_{it}	41	66	62	58	60

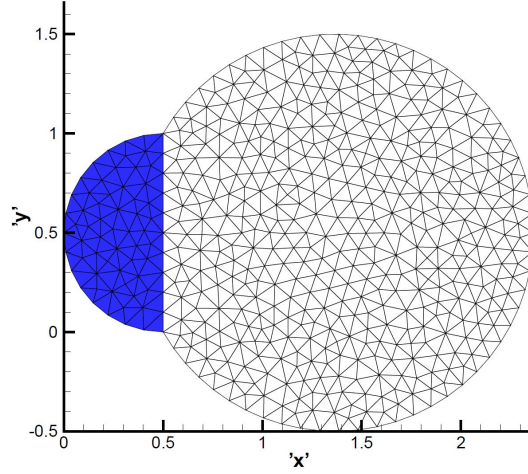


Fig. 5.2. The initial triangular meshes on the half-circle domain for Example 3.

5.4. Example 4: accuracy for general curve interface problem

In the fourth example, we consider the accuracy of the scheme for sinusoid interface problem. The domain $\Omega = (0, 1) \times (0, 1)$ is divided by the interface

$$\Gamma(x) = \frac{1}{2} + \frac{1}{4} \sin(2\pi x)$$

into

$$\Omega_1 = \{(x, y) | x \in (0, 1), y < \Gamma(x)\} \quad \text{and} \quad \Omega_2 = \{(x, y) | x \in (0, 1), y > \Gamma(x)\}.$$

The coefficients are taken to be $\kappa_1 = 2I$ and $\kappa_2 = I$, and the exact solution is taken to be

$$u(x, y) = \begin{cases} -\sin(2\pi x) + e^y, & \text{in } \Omega_1, \\ 2(-\sin(2\pi x) + e^y) + 2, & \text{in } \Omega_2. \end{cases}$$

The interfacial coefficient μ and source term f can be calculated accordingly.

We test this example on random triangular meshes (see Fig. 5.3 for $N_c = 8128$). The mesh size is selected to be $1/8, 1/16, 1/32, 1/64, 1/128$, separately. The numerical result is listed in Table 5.9. We can see that the error of the solution can obtain approximately second order convergence and the convergence order of flux is higher than first order, which shows that our scheme is valid for the general curve interface problems.

Table 5.9: Numerical results for Example 4 on triangular meshes.

N_c	120	496	2004	8128	32656
\mathcal{E}_2^u	3.56E-02	9.79E-03	3.02E-03	8.31E-04	2.30E-04
order		1.86	1.70	1.86	1.85
\mathcal{E}_2^F	1.16E+00	5.42E-01	2.67E-01	1.08E-01	4.87E-02
order		1.09	1.02	1.30	1.15
non_{it}	34	40	44	41	43

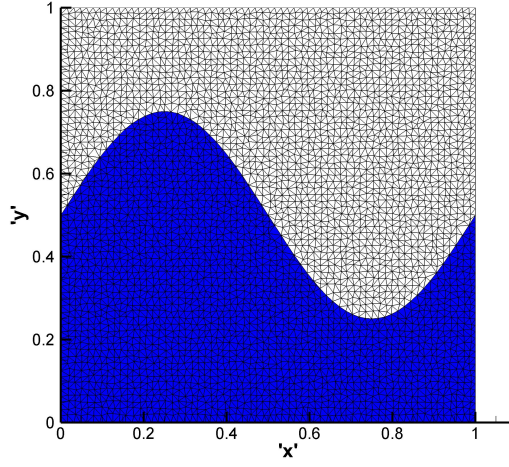


Fig. 5.3. The random triangular meshes of Example 4. ($N_c = 8128$).

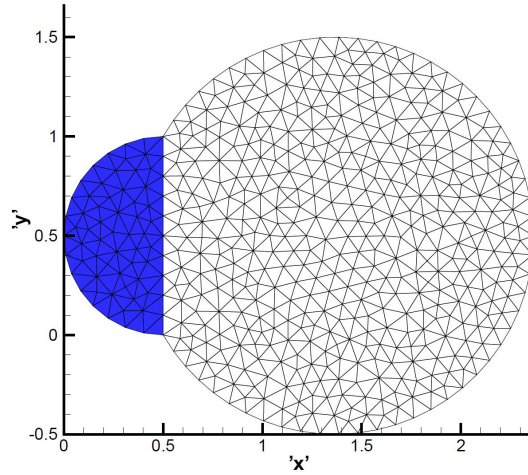


Fig. 5.4. The initial triangular meshes on the half-circle domain for Example 3.

5.5. Example 5: DMP-preserving property under $\mu \equiv 0$

In the fifth example, we verify the DMP-preserving property of our scheme under $\mu \equiv 0$. Take the domain in Example 3 and take $\kappa_1 = R_1 D R_1^T$ and $\kappa_2 = R_2 D R_2^T$, where

$$R_1 = \begin{pmatrix} \cos \theta & -\sin \theta \\ \sin \theta & \cos \theta \end{pmatrix}, \quad R_2 = \begin{pmatrix} \cos \theta & \sin \theta \\ -\sin \theta & \cos \theta \end{pmatrix}, \quad D = \begin{pmatrix} k_1 & 0 \\ 0 & k_2 \end{pmatrix}.$$

We set $\theta = -\frac{5\pi}{12}$, $k_1 = 1 + 2x^2 + y^2$ and $k_2 = 1 + x^2 + 2y^2$ and set the interfacial coefficient $\mu \equiv 0$. The Dirichlet boundary condition is set to be

$$g(x, y) = \begin{cases} x, & \text{on } \partial\Omega_1 \setminus \Gamma, \\ 1 - x, & \text{on } \partial\Omega_2 \setminus \Gamma. \end{cases}$$

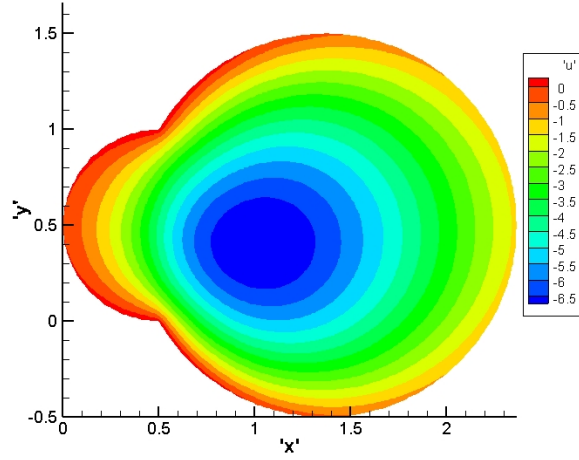


Fig. 5.5. The numerical solution of DMP-preserving scheme of Example 5. ($U_{\min} = -7.0520$, $U_{\max} = 0.5$).

The source term is set to be

$$f(x, y) = \begin{cases} -1, & \text{in } \Omega_1, \\ -100, & \text{in } \Omega_2. \end{cases}$$

The analytical solution of this problem is unknown. According to the maximum principle in Theorem 2.1, the maximum of the exact solution is 0.5.

We apply our scheme to this problem on random triangular meshes, where $N_c = 15200$. The numerical solution is displayed in Fig. 5.5 and the maximum and minimum of numerical solution are 0.5 and -7.0520, respectively. The nonlinear iteration number is 47. The numerical results verify that our scheme is DMP-preserving and robust for $\mu \equiv 0$.

5.6. Example 6: DMP-preserving property under $\mu > 0$

In the last example, we take the domain

$$\Omega_1 = B(O, 1), \quad \Omega_2 = B(O, 2) \setminus B(O, 1), \quad \text{where } O = (0, 0),$$

which is plotted in Fig. 5.6 (a).

We take $\kappa_1 = I$, $\kappa_2 = 10^{14}I$ and the interfacial coefficient $\mu = 1$. The Dirichlet boundary condition on $\partial\Omega_2$ is $g = 1E-10$, and the source term is

$$f(x, y) = \begin{cases} 100, & \text{in } \Omega_1, \\ 0, & \text{in } \Omega_2. \end{cases}$$

We test this example on random triangular meshes (see Fig. 5.6 (a)), where $N_c = 11714$. The solution of DMP-preserving scheme is plotted in Fig. 5.6 (b). The maximum and the minimum on $\bar{\Omega}$ are 75.06 and $1E-10$, respectively, which verifies the DMP-preserving property of our scheme for $\mu > 0$.

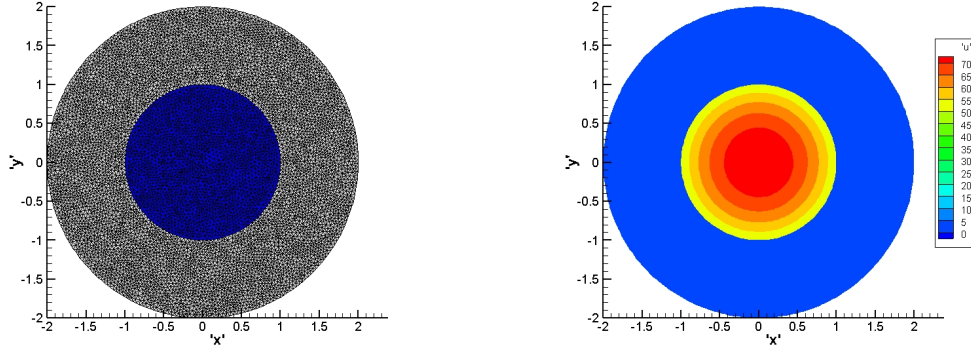
(a) The triangular meshes with $N_c = 11714$.(b) The solution of DMP-preserving scheme.
($U_{\min} = 1\text{E-}10$, $U_{\max} = 75.06$).

Fig. 5.6. The meshes and numerical solution of Example 6.

6. Conclusion

In this paper, we propose a unified finite volume scheme preserving DMP for conjugate heat transfer problems with general interface conditions. The DMP-preserving property and existence of the numerical solution of the proposed scheme are proved. The scheme is valid for non-negative interfacial coefficient on polygonal meshes, and is more general than the scheme proposed in [24] which requires the interfacial coefficient to be strictly positive.

In the numerical experiments, problems with different interfacial coefficients are tested for our scheme and the scheme in [24]. The numerical results show that our scheme obtains second order accuracy for non-negative interfacial coefficient, and the nonlinear iteration numbers do not increase when the interfacial coefficients tend to zero. In contrast, the iteration numbers of scheme in [24] increase rapidly when the interfacial coefficients tend to zero. Especially, the scheme in [24] loses accuracy if there exists a point \mathbf{x}_0 on the interface such that $\mu(\mathbf{x}_0) = 0$. The numerical results show that the proposed scheme is more robust than the scheme in [24]. Furthermore, the second order accuracy and the DMP-preserving property of our scheme are also verified numerically on different shaped interfaces.

Acknowledgments. This work is partially supported by the National Natural Science Foundation of China (11971069,12071045), and the Foundation of CAEP (CX20210042), and Science Challenge Project (No. TZ2016002).

References

- [1] A. Cangiani, E.H. Georgoulis, and Y. A. Sabawi, Adaptive discontinuous Galerkin methods for elliptic interface problems, *Math. Comput.*, **87** (2018), 2675–2707.
- [2] F. Cao, Z. Sheng, and G. Yuan, Monotone finite volume schemes for diffusion equation with imperfect interface on distorted meshes, *J. Sci. Comput.*, **76** (2018), 1055–1077.
- [3] T. Chernogorova, R.E. Ewing, O. Iliev, and R. Lazarov, *Numer. Treat. Multiph. Flows Porous Media*, Springer Berlin Heidelberg, 2000.
- [4] R. Costa, J.M. Nóbrega, S. Clain, and G. J. Machado, Very high-order accurate polygonal mesh finite volume scheme for conjugate heat transfer problems with curved interfaces and imperfect contacts, *Comput. Methods Appl. Mech. Eng.*, **357** (2019), 112560.

- [5] X. He, T. Lin, and Y. Lin, A selective immersed discontinuous Galerkin method for elliptic interface problems, *Math. Methods Appl. Sci.*, **37** (2014), 983–1002.
- [6] H. Huang, J. Li, and J. Yan, High order symmetric direct discontinuous Galerkin method for elliptic interface problems with fitted mesh, *J. Comput. Phys.*, **409** (2020), 109301.
- [7] A. Jain, R. Kanapady, and K. Tamma, Local discontinuous Galerkin method for parabolic problems involving imperfect contact surfaces, *Collection of Technical Papers-44th AIAA Aerospace Sciences Meeting*, **10** (2006), 7076–7086.
- [8] D. Jia, Z. Sheng, and G. Yuan, An extremum-preserving iterative procedure for the imperfect interface problem, *Commun. Comput. Phys.*, **25** (2019), 1–18.
- [9] B.S. Jovanovic, L.D. Ivanovic, and E.E. Suli, Convergence of finite-difference schemes for elliptic equations with variable coefficients, *IMA J. Numer. Anal.*, **7** (1987), 301–305.
- [10] J. Kačur and R. Van Keer, Numerical method for a class of parabolic problems in composite media, *Numer. Methods Partial Differ. Equ.*, **9** (1993), 711–731.
- [11] Z. Li and K. Ito, Maximum principle preserving schemes for interface problems with discontinuous coefficients, *SIAM J. Sci. Comput.*, **23** (2001), 339–361.
- [12] T. Lin, Y. Lin, and X. Zhang, Partially penalized immersed finite element methods for elliptic interface problems, *SIAM J. Numer. Anal.*, **53** (2015), 1121–1144.
- [13] T. Lin, Q. Yang, and X. Zhang, A priori error estimates for some discontinuous Galerkin immersed finite element methods, *J. Sci. Comput.*, **65** (2015), 875–894.
- [14] K. Lipnikov, M. Shashkov, D. Svyatskiy, and Y. Vassilevski, Monotone finite volume schemes for diffusion equations on unstructured triangular and shape-regular polygonal meshes, *J. Comput. Phys.*, **227** (2007), 492–512.
- [15] A.W. Pratt, *Heat transmission in buildings*, Wiley, Chichester, 1981.
- [16] P. Rodrigo, A. Rocha, and M. E. Cruz, Computation of the effective conductivity of unidirectional fibrous composites with an interfacial thermal resistance, *Numer. Heat Transf. Part A Appl.*, **39** (2001), 179–203.
- [17] Z. Sheng and G. Yuan, A nine point scheme for the approximation of diffusion operators on distorted quadrilateral meshes, *SIAM J. Sci. Comput.*, **30** (2008), 1341–1361.
- [18] Z. Sheng and G. Yuan, The finite volume scheme preserving extremum principle for diffusion equations on polygonal meshes, *J. Comput. Phys.*, **230** (2011), 2588–2604.
- [19] L. Wang, S. Hou, and L. Shi, A weak formulation for solving the elliptic interface problems with imperfect contact, *Adv. Appl. Math. Mech.*, **9** (2017), 1189–1205.
- [20] J. Weisz, On an iterative method for the solution of discretized elliptic problems with imperfect contact condition, *J. Comput. Appl. Math.*, **72** (1996), 319–333.
- [21] J. Xu, F. Zhao, Z. Sheng, and G. Yuan, A nonlinear finite volume scheme preserving maximum principle for diffusion equations, *Commun. Comput. Phys.*, **29** (2021), 747–766.
- [22] Q. Yang and X. Zhang, Discontinuous Galerkin immersed finite element methods for parabolic interface problems, *J. Comput. Appl. Math.*, **299** (2016), 127–139.
- [23] G. Yuan and Z. Sheng, Monotone finite volume schemes for diffusion equations on polygonal meshes, *J. Comput. Phys.*, **227** (2008), 6288–6312.
- [24] H. Zhou, Z. Sheng, and G. Yuan, A finite volume method preserving maximum principle for the diffusion equations with imperfect interface, *Appl. Numer. Math.*, **158** (2020), 314–335.
- [25] Q. Zhuang and R. Guo, High degree discontinuous Petrov-Galerkin immersed finite element methods using fictitious elements for elliptic interface problems, *J. Comput. Appl. Math.*, **362** (2019), 560–573.